Steric Control of Luminescence in Phenyl Substituted Trityl Radicals

Petri Murto,[a,b] Biwen Li,[b] Yao Fu,[a] Lucy E. Walker,[a,b] Laura Brown,[a] Andrew D. Bond,[a] Weixuan Zeng,[a] Rituparno Chowdhury,[b] Hwan-Hee Cho,[b] Craig P. Yu,[a,b] Clare P. Grey,[a] Richard H. Friend,[b,*] and Hugo Bronstein[a,b,*]

[a] *Yusuf Hamied Department of Chemistry, University of Cambridge, Cambridge, CB2 1EW, United Kingdom*

[b] *Cavendish Laboratory, University of Cambridge, Cambridge, CB3 0HE, United Kingdom*

*Email: hab60@cam.ac.uk; rhf10@cam.ac.uk

ABSTRACT: Triphenylmethyl (trityl) radicals have shown potential for use in organic optoelectronic applications, but design of practical trityl structures has been limited to donor/radical charge-transfer systems due to the poor luminescence of alternant symmetry hydrocarbons. Here, we circumvent the symmetry forbidden transition of alternant hydrocarbons via excited state symmetry breaking in a series of phenyl substituted tris(2,4,6-trichlorophenyl)methyl (TTM) radicals. We show that threefold phenyl substitution enhances the emission of TTM radical, and that steric control modulates the optical properties in these systems. Simple *ortho*-methylphenyl substitution boosts the photoluminescence quantum efficiency from 1% (for TTM) to 65% at a peak wavelength of 612 nm (for 2-T_3TTM) in solution. In the crystalline solid state, neat 2-T_3TTM radical shows a remarkably high photoluminescence quantum efficiency of 25% for emission peaking at 706 nm. This has implications in the design of aryl substituted radical structures where electronic coupling of the substituents influences variables such as emission, charge transfer and spin interaction.

INTRODUCTION

Neutral π-radicals with an emissive doublet excited state (D_1) are of interest for applications in photonics and light-emitting devices[1-4] and magnetically and optically addressable quantum systems[5-8] because of the absence of energetically low-lying non-emissive states in these materials. Chlorinated triphenylmethyl (trityl) radicals like tris(2,4,6-trichlorophenyl)methyl (TTM) are among the most studied spin doublet systems largely because of their remarkable stability up to years under ambient air.[9-10] Previously, trityl radicals had been classified dark with photoluminescence quantum efficiencies (PLQEs) not higher than few percent.[11-15] This is because their alternant symmetry structure gives rise to an energetically symmetric splitting of occupied and unoccupied molecular orbitals with a distinction that only their sign is opposite relative to the non-bonding, singly occupied molecular orbital (SOMO), as illustrated in Figure 1. This in turn translates to degenerate highest occupied molecular orbital to singly occupied molecular orbital (HOMO–SOMO) and singly occupied molecular orbital to lowest unoccupied molecular orbital (SOMO–LUMO) transitions and equal dipole moments resulting in a vanishing oscillator strength for the lowest-energy (D_0–D_1) excitation in these structures.[16-18] To brighten up radicals, the key is to lift the degeneracy of these transitions. Much enhanced emission has been obtained from charge-transfer (CT) systems where the radical has been covalently coupled to non-alternant hydrocarbon structures like carbazole with a nitrogen heteroatom introducing a non-bonding, lone electron pair to the π-system.[19-22]

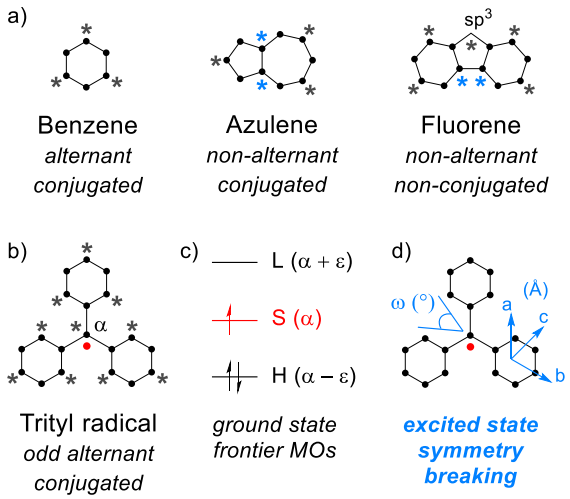

Figure 1. a) Examples of alternant and non-alternant hydrocarbons where sp^2 hybridized carbon atoms are marked with black dots. In an alternant system, conjugated atoms can be divided into two sets, starred and unstarred, such that no two atoms in the same set are directly linked to one another. b) In trityl radical, alternant symmetry is achieved in an odd number of conjugated atoms due to the half-filled molecular orbital at the α-carbon. Red dot represents radical electron. c) Schematic ground state frontier molecular orbital diagram of trityl radical where the occupied and unoccupied molecular orbitals are separated from the half-filled molecular orbital by an equal but opposite energy, $-\varepsilon$ and $+\varepsilon$, respectively (S, SOMO; H, HOMO; L, LUMO). Electron occupancy is shown by half-headed arrows. d) Illustration of changes in dihedrals and bond lengths that can lead to reduced, broken symmetry in the excited state of trityl radical.

Contrary to the previous knowledge, we have recently introduced an alternative approach where symmetric radicals can be made emissive if their symmetry is broken in the excited state.[23] Similar observations have been made in some substantially bulky aryl substituted trityl radicals suggesting that excited state symmetry breaking may be sterically controlled.[24-27] However, the extent of symmetry breaking in radical emitters is not commonly understood nor thoroughly studied, and for this one may take the advantage of asymmetric changes in dihedrals and bond lengths, that is, perturbation of the lowest-energy electronic transitions in the π-systems (Figure 1d). Significant progress in this regard

would greatly expand the design of luminescent radical materials, both those of alternant symmetry structures and those of CT type non-alternant hydrocarbon structures.

Herein, we report a systematic series of phenyl substituted TTM radicals with varied degrees of steric bulk. Introduction of methyl groups to the phenyl rings mixes their molecular orbital energy structure as illustrated in Figure S1, whereas SOMO associated with the radical centre remains energetically unchanged (Figure S2). Coupling these phenyl substituents from different positions to TTM allows building a family of radicals whose luminescence is controlled both sterically and electronically. Similar modification of phenyl ligands by methyl groups has been demonstrated to affect the ground state spin structure of organometallic (non-radical) spin-optical interfaces.[28-29] We show that subtle changes in sterics can significantly influence the luminescence in spin radicals and that their PLQEs do not strictly follow the energy gap law.[30]

Scheme 1. Synthesis of phenyl substituted radical derivatives

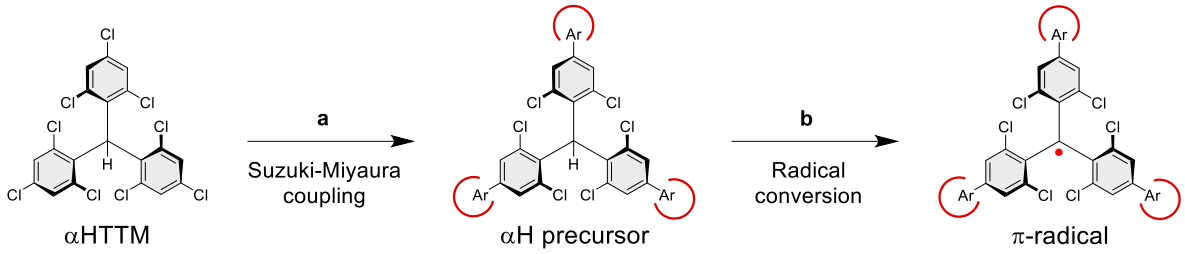

[a] $ArB(OH)_2$ (6 equiv.), $Pd(OAc)_2$ (0.02 equiv.), SPhos (0.04 equiv.), K_3PO_4 (9.6 equiv.), 1,4-dioxane, 80 °C, 24 h.
[b] 1) Bu_4NOH (aq., 2 equiv.), THF/DMSO 1:3, RT, 4 h; 2) *p*-chloranil (2.5 equiv.), RT, 1 h.

Table 1. Summary of the synthesized radicals and their photophysical parameters

Radical	Ar group	Yield, **a**/**b** (%)[a]	λ_{abs}, soln (nm)[b,c]	λ_{PL}, soln (nm)[b,d]	Φ_{PL}, soln (%)[b,e]	τ_{PL}, soln (ns)[b,f]	k_r, soln ($\times10^6$ s^{-1})[b,g]	k_{nr}, soln ($\times10^6$ s^{-1})[b,h]
P_3TTM		38/74	408, 541	643	29	9.3	30.9	76.1
4-T_3TTM		38/80	413, 555	651	36	8.6	41.9	73.8
3-T_3TTM		72/72	410, 545	646	22	8.7	25.5	89.8
2-T_3TTM		78/79	389, 543	612	65	25.5	25.4	13.8
3,5-X_3TTM		59/63	411, 548	649	22	8.0	27.7	97.3
2,6-X_3TTM		67/69	377, 536	583	13	23.2	5.5	37.5
2,5-X_3TTM		89/86	390, 543	615	45	23.1	19.4	23.8
2,4-X_3TTM	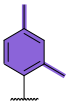	57/90	395, 538	621	55	22.2	24.8	20.2
M_3TTM	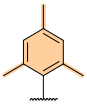	15/86	374, 537	590	23[i]	28.1[i]	8.2[i]	27.4[i]
2,6-ipP_3TTM	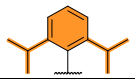	15/85	378, 540	578	5	10.5	4.5	90.9

[a] Isolated yields for synthetic steps **a** and **b** shown in Scheme 1. [b] Sample in 0.1 mM toluene solution. [c] Highest- and lowest-energy peaks of UV-vis absorption. [d] Photoluminescence peak wavelength. [e] Photoluminescence quantum efficiency. [f] Photoluminescence lifetime. [g] Radiative decay rate. [h] Nonradiative decay rate. [i] Obtained from ref.[23]

RESULTS AND DISCUSSION

The phenyl substituted radicals were obtained via Suzuki–Miyaura (S–M) coupling of αHTTM and the respective arylboronic acid ($ArB(OH)_2$) in mild anhydrous conditions,[31] followed by radical conversion through deprotonation and one-electron oxidation, as outlined in Scheme 1. Detailed synthetic procedures and structural characterization are described in the Supporting Information (SI). We find that anhydrous S–M reaction conditions in a polar environment (1,4-dioxane) with SPhos ligand give αH precursor molecules without *ortho*-dehalogenation,[23] and that solubility of these products is affected by their polarity. The yields of the threefold S–M couplings reported in Table 1 are those of isolated products, and they reflect both steric bulk of the aryl substituents and solubility of the αH precursor derivatives rather than reactivity of the *para*-chlorines in these reactions. Radical conversion benefits from a highly polar environment that stabilizes the highly soluble anionic equilibrium intermediate, so that the reaction reaches completion after the oxidation step giving high yields throughout the series.

Starting from phenyl substituted P_3TTM radical, we introduced methyl groups to the *ortho*-, *meta*- and *para*-positions of methylphenyl (tolyl) substituted 2-T_3TTM, 3-T_3TTM and 4-T_3TTM radicals, respectively. The position of the methyl groups was varied on the merit of controlling 1) π-conjugation between the phenyl rings and the TTM radical and 2) inductive effect of the electron-donating methyl groups. Both factors are anticipated to influence the electron-donating strength of the phenyl rings and, thus, the CT contribution of electronic transitions in these radicals. Varied steric bulk between the phenyl rings and the TTM chlorophenyl rings would affect the molecular symmetry of the radicals in ground and optically excited states. We extended the series through 2,4-, 2,5-, 2,6- and 3,5-dimethylphenyl (xylyl) substituted radicals 2,4-X_3TTM, 2,5-X_3TTM, 2,6-X_3TTM and 3,5-X_3TTM, respectively, to 2,4,6-trimethylphenyl (mesityl) substituted M_3TTM. Finally, the steric bulk was increased with two isopropyl groups in 2,6-ipP_3TTM radical, while still obtaining a reasonable yield

in the threefold S–M coupling. Significantly lower yields were obtained with any bulkier groups in the phenyl ring. In this way a comprehensive, new series of phenyl substituted radical derivatives was synthesized for photophysical studies.

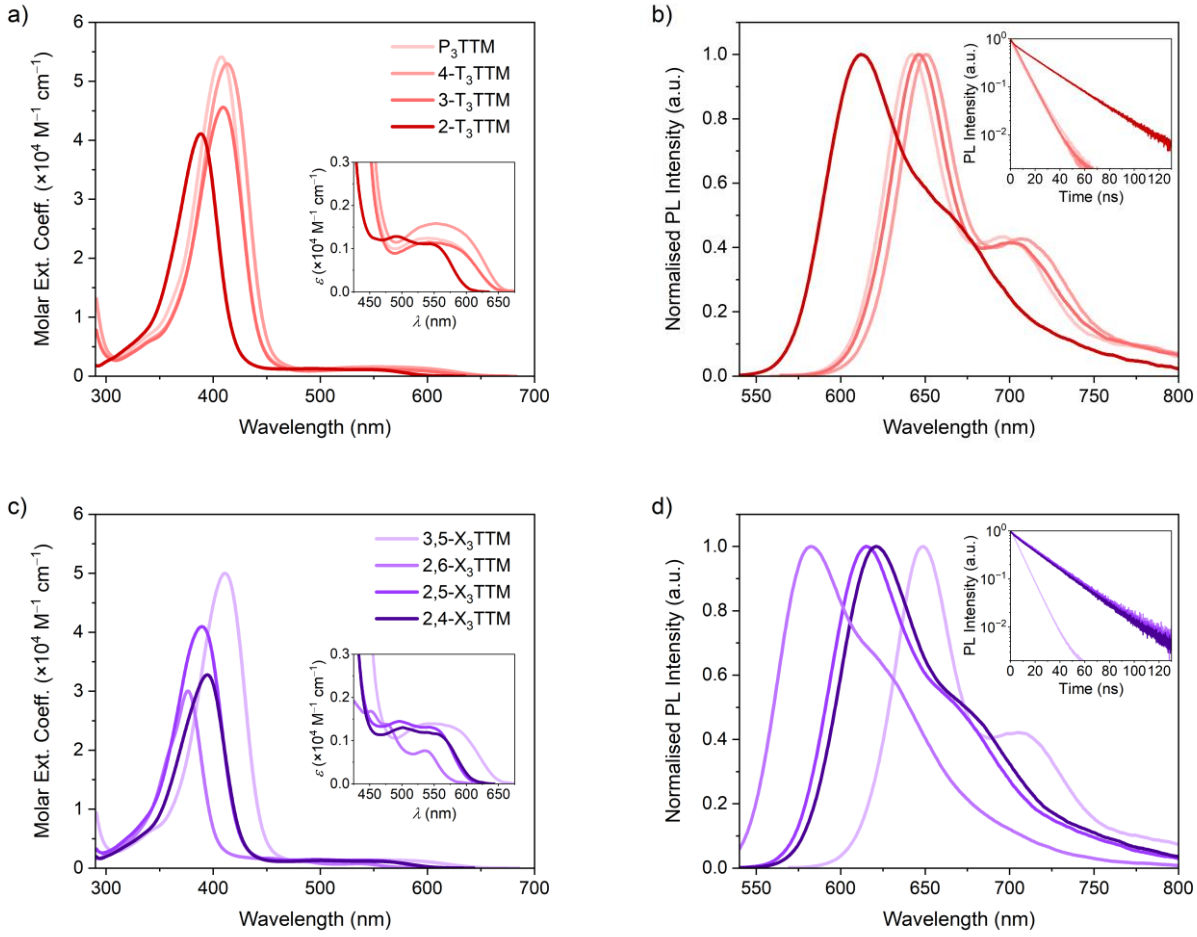

Figure 2. a,c) Optical absorption and b,d) photoluminescence spectra of radicals following 520 nm excitation in 0.1 mM toluene solution. The insets in a,c) show close-ups of the low-energy absorption region and the insets in b,d) show total emission kinetics.

Figure 2 shows optical absorption and photoluminescence spectra of the synthesized radicals and the photophysical parameters are summarized in Table 1. Excitation spectra and the corresponding spectra for M_3TTM and 2,6-ipP_3TTM are included in Figure S3. We observe that the absorption spectra are generally redshifted with decreasing steric bulk due to effective conjugation between the phenyl rings

and the radical centre, whereas *para*-methyls serve to somewhat strengthen the lowest-energy D_0–D_1 transition suggesting stronger CT contribution in both tolyl and xylyl substituted systems. Emission of tolyl substituted radicals (Figure 2b) is systematically redshifted following the effects of conjugation and CT character in line with their absorption profiles. It is remarkable that phenyl substitution switches the dark TTM radical emissive with an increase of PLQE from 1% (for TTM) to 29% (for P_3TTM) while redshifting the emission from 568 to 643 nm in toluene solution, respectively.[23] This is unexpected on the basis of molecular symmetry and lack of steric bulk, and reasons to the emission enhancement are discussed later in this manuscript. We find a trend in increasing PLQE in the order 3-T_3TTM < P_3TTM < 4-T_3TTM < 2-T_3TTM, which stem from the nonradiative decay rates being suppressed in the same order and further from decreasing changes between ground and excited state conformations following our computational study (vide infra). Emission is enhanced with a *para*-methyl and even more so with an *ortho*-methyl coupled to the phenyl ring. 2-T_3TTM stands out as the most emissive radical in this series and its PLQE of 65% at a peak wavelength of 612 nm compares to those of many state-of-the-art CT emitters that are based on non-alternant donor–acceptor type radical design.[20-21,32-33]

Interplay between sterics and CT contribution become prominent in the emission of xylyl substituted radicals (Figure 2d). Increased steric bulk in 2,6-X_3TTM renders the radical poorly emissive and this is further pronounced in 2,6-ipP_3TTM. On the other hand, *meta*-methyls show minimal effect on emission wavelengths, kinetics and PLQEs as observed in comparison of 3-T_3TTM and 3,5-X_3TTM radicals. 2,4-X_3TTM and 2,5-X_3TTM can be described as intermediate structures where CT contribution is enhanced more by the *para*-methyls than by the *meta*-methyls, respectively, leading to stronger and redshifted emission in the former radical.

Emission in PMMA doped films resembles that in solution, but we observe stronger vibronic features (Figure S4a,b). The peak wavelengths are redshifted by less than 10 nm throughout the series confirming that emission in these radicals is dominated by changes in their substitution pattern, but also suggesting that symmetry can be broken in the solid state due to changes in conformation, as observed in structurally related triphenylphosphine radicals.[34] In the crystalline solid state, emission is systematically quenched with reducing steric bulk due to increasing aggregation (Figure S4c,d and Table S1). However, 2-T_3TTM breaks this pattern and delivers the highest PLQE in this series, 25% at a peak wavelength of 706 nm, that is, for a neat radical that has not been diluted into any host matrix. Higher PLQEs have only been obtained from co-crystals of radicals doped in their corresponding αH precursors,[35-36] whereas the redshifted emission of neat 2-T_3TTM can be ascribed to that of an excimer.[37-38] These results indicate that ideal steric bulk maintains effective conjugation between the phenyl substituents and the radical centre while still allowing symmetry breaking, as developed below.

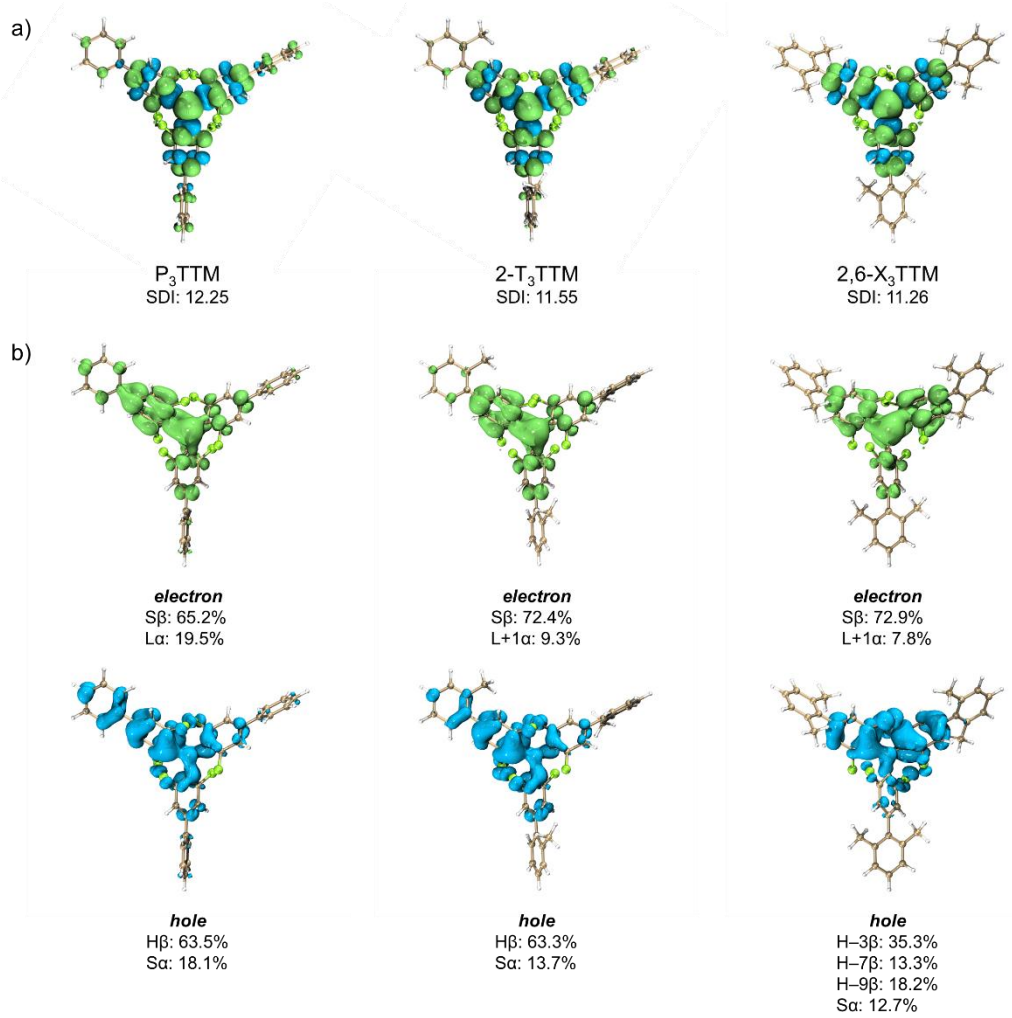

Figure 3. a) Visualization of electron spin density for computationally optimized D_0 state geometries of P_3TTM, 2-T_3TTM and 2,6-X_3TTM and b) hole-electron analysis for vertical excited state based on their D_0 geometries (S, SOMO; H, HOMO; L, LUMO).

Quantum-chemical modelling was employed to better understand the optical properties of the phenyl substituted radicals. It is apparent from the geometry-optimized ground state structures that positioning of the methyl groups leads to different in-phase and out-of-phase combinations of frontier molecular orbitals between the outer phenyl rings and the radical centre (Section S4). Particularly, structures with the highest occupied molecular orbitals in-phase, e.g., P_3TTM and 2-T_3TTM show higher oscillator strength for the lowest-energy D_0–D_1 excitation than the ones with the corresponding orbitals out-of-phase, e.g., 2,6-X_3TTM (similar trend is observed experimentally in Figure 2a,c). In the former case

vertical excitation takes place primarily from the highest (doubly) occupied molecular orbital of the phenyl substituent to the singly occupied molecular orbital of the radical (HOMO–SOMO transition), whereas in the latter case the transition is a result of a mixture of contributions from deeper-energy HOMOs around the radical centre, as illustrated by the hole-electron analysis in Figure 3b. Moreover, isolation of the outer phenyl rings due to increasing steric bulk is observed as localization of electron spin density on the TTM core (Figure 3a), which is expressed numerically as decreasing spatial delocalization index (SDI) in Figure 4c.

Our calculations suggest that both *ortho*- and *para*-methyls increase the oscillator strength of vertical and adiabatic D_1 states relative to P_3TTM due to enhanced phenyl-to-radical charge transfer (Table S4). This effect is cancelled out in 2,6-X_3TTM as a result of steric bulk and poor orbital overlap, as discussed above. Generally, electronic transitions are localized between the radical centre and one of the three outer phenyl rings. The corresponding phenyl-phenyl arm becomes co-planar and the sp^2–sp^2 single bond shortens in the adiabatic D_1 state suggesting that excited state symmetry breaking operates in all threefold aryl substituted radicals regardless of their steric bulk (Table S3). This has not been observed previously in trityl radicals. Structures without *ortho*-methyls are relatively co-planar already in the ground state, whereas those with two *ortho*-methyls remain twisted also in the D_1 state and their phenyl-phenyl bond lengths remain the most single bond-like in this series (in the former case the experimental photoluminescence spectra are more structured, Figure 2b,d). 2-T_3TTM, 2,4-X_3TTM and 2,5-X_3TTM with one *ortho*-methyl stand in the middle resulting in smallest change between ground and excited state dihedrals, 15.8, 17.3 and 17.2°, respectively, and highest oscillator strength for the adiabatic D_1 state, which in part explain the low experimental nonradiative decay rates in these three systems. We also find that *ortho*-methyls provide significant energy barrier for planarization minimizing chances for rotation past co-planar conformation (Figure S5). Population of different conformations within these limits is illustrated by Boltzmann distribution for each structure in Figure

4c, where *ortho*-methyls control rotational freedom and thereby effective conjugation between the phenyl ring and the radical centre.

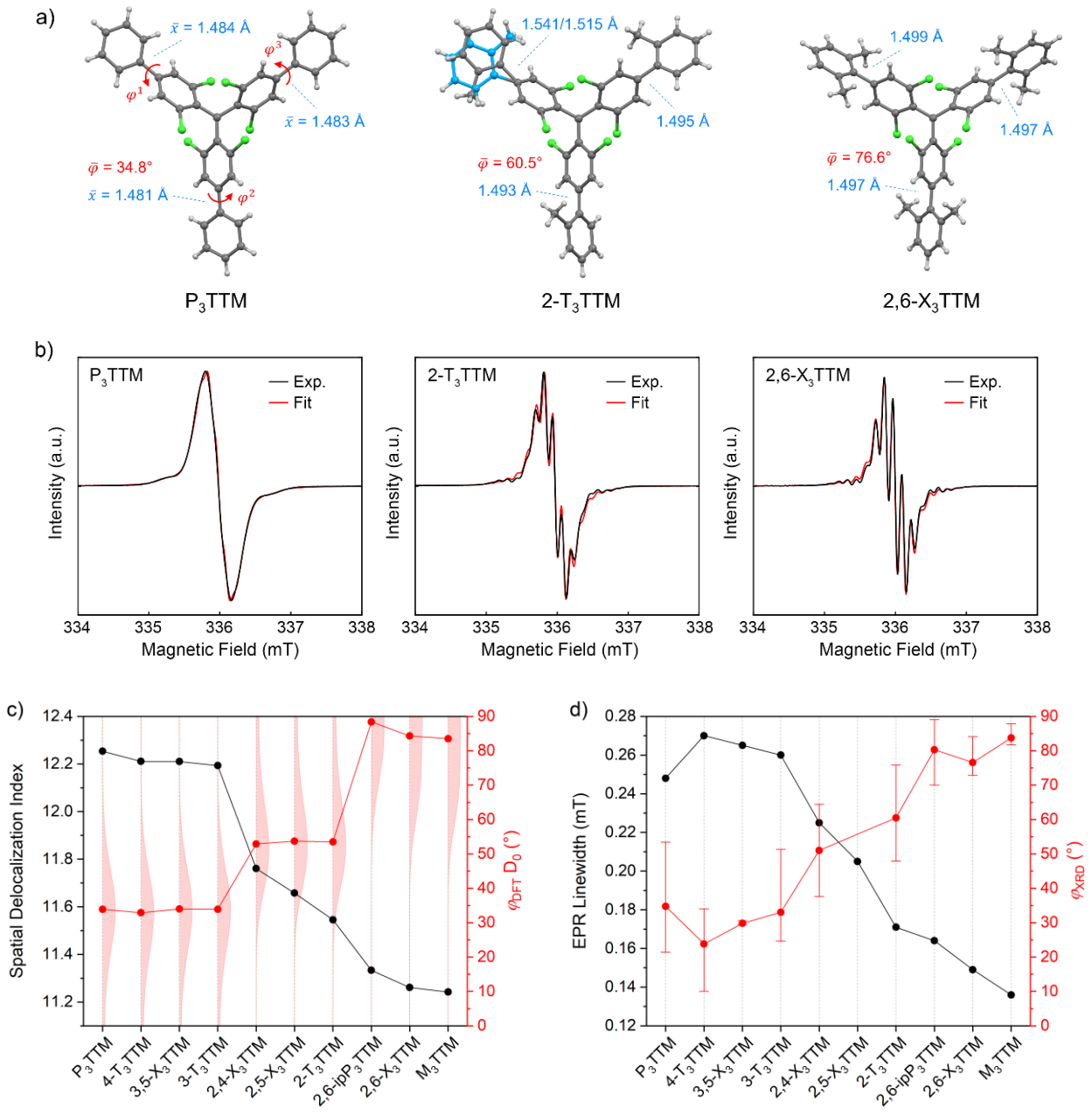

Figure 4. a) Molecular structures from X-ray crystal structures of the synthesized P_3TTM, 2-T_3TTM and 2,6-X_3TTM radicals with average phenyl-phenyl dihedrals (red) and single bond lengths (blue). In the structure of 2-T_3TTM, carbon atoms in blue highlight 2-fold rotational disorder of the phenyl ring. b) Continuous-wave X-band EPR spectra for the radicals measured at 200 K in 1 mM toluene solution (black) and simulated spectra (red) with fit parameters given in Table S9. c) Computational

spatial delocalization index for electron spin density (black symbols) and dihedrals for aryl group Ar^1 in different radical structures in their optimized D_0 state (red symbols) with rotational freedom illustrated by Boltzmann distribution at 298.15 K (red filled curves, the thinnest part stands for minimum and the thickest part for maximum population). d) Experimental peak-to-peak linewidth in the EPR spectra (black symbols) and average phenyl-phenyl dihedrals in the X-ray crystal structures (red symbols). The red intervals represent variation between minimum and maximum torsion in these structures. A crystal structure could not be determined for 2,5-X_3TTM (see Section S6).

Molecular structures from X-ray crystallography show further evidence of changes in conformation in the synthesized radicals (Figure 4a,d). For molecules without *ortho*-methyls a wide range of dihedrals is observed between 10.0–53.4°, whereas for those with one *ortho*-methyl the range is shifted upwards between 37.6–75.9°. In molecules with two *ortho*-methyls the distribution is narrowed near orthogonal between 70.0–89.0°. These experimental observations fit well into the population distributions of the computational models shown in Figure 4c. Crystal structures and average phenyl-phenyl dihedrals and bond lengths for P_3TTM, 2-T_3TTM and 2,6-X_3TTM are included in Figure 4a, which shows apparent disorder of the orientation of one of the phenyl rings in 2-T_3TTM (see Section S6 for further discussion). Simulation of these structures suggests that electronic transitions in a monomolecular level resemble those of our computational models (Table S5), further indicating that the observed redshifted emission in the crystalline solid state comes from an excimer (Figure S4 and Table S1).

Electron paramagnetic resonance (EPR) spectroscopy provides valuable insight into the environment of the unpaired electron in the synthesized molecules. Figure 4b shows experimental spectra for P_3TTM, 2-T_3TTM and 2,6-X_3TTM recorded in 1 mM toluene solution at 200 K. The distinct spectral feature observed in these compounds is EPR peak-to-peak linewidth. The broad septet band in 2-T_3TTM and the narrow septet splitting in 2,6-X_3TTM are due to isotropic hyperfine coupling between

the radical electron and the closest six aromatic hydrogens in the TTM structure (labelled δ/δ' hydrogens in Table S9). In the case of P_3TTM, the septet band appears considerably broader and less resolved. Upon analysing the EPR spectra for all radicals in this study (Figure 4b and Figure S7), we find that the g-factor remain consistent (g = 2.0156) and there are slight variations in the hyperfine coupling constants with the aromatic hydrogens. Since the similarity in these parameters does not account for the differences observed in peak linewidths, we hypothesize the peak linewidths are influenced by molecular motion, and the dynamic averaging resulting from conformational flexibility may lead to narrower peak widths.[39] To quantify this, we have extracted peak-to-peak linewidths through fitting,[40-41] and the parameters are summarized in Table S9. Figure 4d illustrates a systematic decrease in linewidth as the steric bulk increases around the TTM core, indicating more conformational flexibility as the radical becomes less conjugated, in good agreement with the computational spin delocalization shrinking in the same order (Figure 4c). Overall, fine changes in steric bulk and electronic coupling of the phenyl rings are observed as greatly enhanced luminescence in 2-T_3TTM as indicated by both computational and experimental analyses.

CONCLUSIONS

In conclusion, sterics play various roles in the emission of TTM radical. We show that excited state symmetry breaking is a general phenomenon that operates in threefold aryl substituted radicals, and that luminescence can be boosted by controlling the steric bulk in these structures. Sterics also dictate the inductive effect of the aryl substituents. Specifically, *ortho*-methylphenyl substituted 2-T_3TTM stands as a prime example where the phenyl ring is coupled in-phase to the radical and symmetry breaking is achieved with minimal change in excited state conformation, resulting in suppression of nonradiative decay channels, and thus photoluminescence quantum efficiency of 65% is achieved at a peak wavelength of 612 nm in solution. The same design motif holds in the solid state, and neat crystals of 2-T_3TTM maintain a photoluminescence quantum efficiency of 25% at a peak wavelength of 706 nm. This study demonstrates that steric control of electronic coupling in aryl substituted radicals can

be used as an effective method to design highly luminescent spin systems based on alternant symmetry structures and, by analogy, non-alternant hydrocarbon structures. The relevant question is from which position these substituents are coupled to the radical.

EXPERIMENTAL METHODS

Characterization and techniques. NMR spectra were recorded on a 400 MHz Bruker Avance III HD spectrometer (^{1}H, 400 MHz; ^{13}C, 100 MHz). Chemical shifts are reported in δ (ppm) relative to the solvent peak: chloroform-*d* ($CDCl_3$: ^{1}H, 7.26 ppm; ^{13}C, 77.16 ppm) and dichloromethane-d_2 (CD_2Cl_2: ^{1}H, 5.32 ppm; ^{13}C, 53.84 ppm). Mass spectra were obtained on a Waters Xevo G2-S benchtop QTOF mass spectrometer using electrospray ionization (ESI) or an atmospheric solids analysis probe (ASAP). C, H, N combustion elemental analyses were obtained on an Exeter Analytical Inc. CE-440 elemental analyser and the results are reported as an average of two samples. Flash chromatography was carried out using Biotage® Isolera™ Four System and Biotage® SNAP/Sfär Silica flash cartridges.

Optical absorption and photoluminscence spectroscopy. UV-visible spectra were measured with a commercially available Shimadzu UV-1800 spectrophotometer. Steady-state photoluminescence and excitation spectra of samples in solution were measured with a commercially available Edinburgh Instruments FS5 Spectrofluorometer system using xenon lamp as the light source. Photoluminescence of crystalline solid-state samples were measured with the same instrument and PLQEs were obtained using an integrating sphere and an excitation wavelength of 405 nm. The measurements were carried out by placing vacuuum-dried single crystals between two glass plates (preparation of the crystals is described in the experimental section for X-ray crystallography). Photoluminescence of samples in PMMA films were measured in a home-built setup by providing a continuous wave excitation at 405 nm using a diode laser. Photoluminscence was collected in a reflection mode setup after passing photons through a 450 nm long-pass filter (Thor Labs). Transmitted photons were collected in a

collimating 2-lens apparatus and directed into an optical fiber which supplied the photons into a calibrated grating-spectrometer (Andor SR-303i) and finally into a Si-camera where they were recorded. Output spectra were corrected taking into account the filter transmission and camera sensitivity. PLQE measurements of samples in solution and PMMA films were performed using an integrating sphere and samples were excited by a continuous-wave 405 nm laser. The laser and sample emission signals were measured by a calibrated grating spectrometer (Andor SR-303i) using a Si detector. Time resolved single photon counting using timing electronics (TimeHarp260) was carried out by irradiating the samples with an electrically pulsed 407 nm laser using a function generator at a frequency of 5–10 MHz providing a time resolution of up to 200 ns. Photons emitted from the sample were passed through a 450 nm long-pass filter (Thor Labs Ltd.) to remove laser scatter. Subsequently transmitted photons were collected by a Si-based single-photon avalanche photodiode. All spectroscopy was carried out under ambient air.

Cyclic voltammetry. Cyclic voltammetry was carried out on a PalmSens EmStat4S potentiostat in a three-electrode setup using a glassy carbon (GC) electrode (3.0 mm diameter) as the working electrode (WE), platinum wire as the counter electrode (CE) and freshly activated silver wire as the Ag/Ag^+ reference electrode (RE). The silver wire was activated by immersing in concentrated HCl solution to remove any silver oxides or other impurities, then rinsed with water and acetone and dried prior to each measurement. The RE was calibrated against ferrocene/ferrocenium (Fc/Fc^+) redox couple at the end of each measurement (the Fc/Fc^+ half-wave potential, $E_{1/2}$, was determined at 0.20 V vs. Ag/Ag^+). The supporting electrolyte was 0.1 M solution of Bu_4NPF_6 in anhydrous THF and the scan rate was 0.1 V s^{-1}. The electrolyte was bubbled with Ar gas before each measurement to remove any dissolved oxygen. Sample concentration was in the order of 10^{-5} M.

DFT calculations. Density functional theory (DFT) calculations were performed using Gaussian 16 program. Ground state geometries were optimized at unrestricted UB3LYP/def2-SVP level (for radicals) or at restricted B3LYP/def2-SVP level (for aryl groups). Dispersion correction was conducted by Grimme's D3 version.[42] Potential energy surfaces were scanned as a function of dihedral for aryl group Ar^1 at steps of 5° by optimizing the structure to the energy minimum at each step and using the same unrestricted functional and basis set. Boltzmann distributions were calculated from these potential energy scans at 298.15 K. Basing on the optimized ground state geometries, vertical excitation energies were evaluated at UPBE0/def2-TZVP by time-dependent DFT (TD-DFT) treatment. The D_1 state geometries were optimized at UPBE0/def2-SVP level and the adiabatic D_1 state energies were evaluated using the same functional but basis set of def2-TZVP. For comparison, excited state analysis was also carried out with the UM06-2X functional,[43] while using same basis sets at each step as described for the UPBE0 functional. The numerical data in Table S4 shows that both methods give similar trends that follow the experimental observations, but with a difference that UPBE0 better reproduces the experimental energies and oscillator strengths, and it is therefore selected as the representative method in this study. Following these results, excited state analysis of molecular structures from X-ray crystallography was carried out in two steps: first, all hydrogen atom positions were optimized at UB3LYP/def2-SVP level by freezing all carbon atoms to the X-ray crystal structure geometry and, second, vertical excitation energies of these structures were calculated by TD-DFT at UPBE0/def2-TZVP level. Spatial delocalization indexes and excited state analysis were processed using the Multiwfn 3.8 program according to the program manual and literature method.[44] Visualization of the optimized structures was done using the Visual Molecular Dynamics 1.9.3 (VMD) software.[45]

EPR spectroscopy. EPR experiments were conducted using an X-band benchtop EPR spectrometer (E5000, Magnettech), operating at a microwave frequency of 9.47 GHz and a temperature of 200 K,

regulated by a variable-temperature unit. A modulation field of 0.02 mT was applied at a modulation frequency of 100 kHz with a microwave power of 5 mW. For sample preparation, all samples were dissolved in toluene at a concentration of 1 mM and then transferred into glass capillaries with a 1 mm diameter (Bruker), which were subsequently sealed with Critoseal. EasySpin software was employed to simulate the EPR spectra.[46]

X-Ray crystallography. Crystals were prepared by dissolving the sample in DCM in an NMR tube and either MeOH or EtOH was added on top as an antisolvent, and the solvents were allowed to mix slowly in the dark. Single-crystal X-ray diffraction data were collected on a Bruker D8-QUEST diffractometer, equipped with an Incoatec IμS Cu microsource (λ = 1.5418 Å) and a PHOTON-III detector operating in shutterless mode. The temperature was controlled at 180(2) K using an Oxford Cryosystems open-flow N_2 Cryostream. The control and processing software was Bruker *APEX4*. The diffraction images were integrated using *SAINT* in *APEX4* and a multi-scan correction was applied using *SADABS*. The final unit-cell parameters were refined against all reflections over the full data range. Structures were solved using *SHELXT*[47] and refined using *SHELXL*.[48] Full details of the crystallographic refinements are provided in the SI. The crystal structures were visualized using the Mercury 2021.3.0 software.[49-50]

ASSOCIATED CONTENT

Data Availability Statement

Optical absorption and photoluminescence spectra, emission kinetics, computational atomic coordinates of optimized ground and excited state structures, and EPR spectra are openly available in the University of Cambridge Repository at https://doi.org/10.17863/CAM.107368. All other data underlying this study are available in the published article and its Supporting Information.

Supporting Information

The Supporting Information is available free of charge at https://pubs.acs.org/doi/

Supporting figures, synthetic procedures and structural characterization, additional optical spectra, computational structures and data, cyclic voltammetry, X-ray crystallographic structures, refinements and data, EPR spectra and data, and NMR spectra (PDF).

Accession Codes

CCDC 2305967, 2305968, 2305969, 2305970, 2305971, 2305972, 2305973 and 2305974 contain the supplementary crystallographic data for this paper. These data can be obtained free of charge via www.ccdc.cam.ac.uk/data_request/cif, or by emailing data_request@ccdc.cam.ac.uk, or by contacting The Cambridge Crystallographic Data Centre, 12 Union Road, Cambridge CB2 1EZ, United Kingdom; fax: +44 1223 336033.

AUTHOR INFORMATION

Corresponding Authors

Hugo Bronstein – *Yusuf Hamied Department of Chemistry, University of Cambridge, Cambridge CB2 1EW, United Kingdom*; *Cavendish Laboratory, University of Cambridge, Cambridge CB3 0HE, United Kingdom*; orcid.org/0000-0003-0293-8775; Email: hab60@cam.ac.uk

Richard H. Friend – *Cavendish Laboratory, University of Cambridge, Cambridge CB3 0HE, United Kingdom*; orcid.org/0000-0001-6565-6308; Email: rhf10@cam.ac.uk

Authors

Petri Murto – *Yusuf Hamied Department of Chemistry, University of Cambridge, Cambridge CB2 1EW, United Kingdom*; *Cavendish Laboratory, University of Cambridge, Cambridge CB3 0HE, United Kingdom*; orcid.org/0000-0001-7618-000X

Biwen Li – *Cavendish Laboratory, University of Cambridge, Cambridge CB3 0HE, United Kingdom*

Yao Fu – *Yusuf Hamied Department of Chemistry, University of Cambridge, Cambridge CB2 1EW, United Kingdom*; orcid.org/0000-0003-4103-0065

Lucy E. Walker – *Yusuf Hamied Department of Chemistry, University of Cambridge, Cambridge CB2 1EW, United Kingdom*; *Cavendish Laboratory, University of Cambridge, Cambridge CB3 0HE, United Kingdom*; orcid.org/0009-0009-8149-8034

Laura Brown – *Yusuf Hamied Department of Chemistry, University of Cambridge, Cambridge CB2 1EW, United Kingdom*

Andrew D. Bond – *Yusuf Hamied Department of Chemistry, University of Cambridge, Cambridge CB2 1EW, United Kingdom*; orcid.org/0000-0002-1744-0489

Weixuan Zeng – *Yusuf Hamied Department of Chemistry, University of Cambridge, Cambridge CB2 1EW, United Kingdom*; orcid.org/0000-0003-1577-9021

Rituparno Chowdhury – *Cavendish Laboratory, University of Cambridge, Cambridge CB3 0HE, United Kingdom*; orcid.org/0000-0003-3063-4576

Hwan-Hee Cho – *Cavendish Laboratory, University of Cambridge, Cambridge CB3 0HE, United Kingdom*; orcid.org/0000-0002-2205-729X

Craig P. Yu – *Yusuf Hamied Department of Chemistry, University of Cambridge, Cambridge CB2 1EW, United Kingdom*; *Cavendish Laboratory, University of Cambridge, Cambridge CB3 0HE, United Kingdom*; orcid.org/0000-0002-1423-5244

Clare P. Grey – *Yusuf Hamied Department of Chemistry, University of Cambridge, Cambridge CB2 1EW, United Kingdom*; orcid.org/0000-0001-5572-192X

Complete contact information is available at:

https://pubs.acs.org/doi/

Funding

P.M., W.Z. and R.C. have received funding from the European Union's Horizon 2020 research and innovation programme under the Marie Skłodowska-Curie grant agreements No. 891167, No. 886066 and No. 859752. R.H.F., P.M., L.W. and H.-H.C. acknowledge funding from the European Research Council under the European Union's Horizon 2020 research and innovation programme grant agreement No. 101020167. Y.F., C.P.G and H.B. were supported by the Engineering Physical Sciences Research Council (EPSRC, EP/W017091/1 Programme Grant and EP/S003126/1). C.P.Y. thanks the Herchel Smith Fund for the Herchel Smith postdoctoral fellowship award at the Yusuf Hamied Department of Chemistry, University of Cambridge.

Notes

The authors declare no competing financial interest.

ACKNOWLEDGEMENTS

We thank Dr Dijana Matak-Vinkovic, Dr Roberto Canales and Asha Boodhun for carrying out the mass spectrometry and Dr Nigel Howard for carrying out the elemental analyses at the Yusuf Hamied Department of Chemistry, University of Cambridge.

REFERENCES

1. Hudson, J. M.; Hele, T. J. H.; Evans, E. W., Efficient light-emitting diodes from organic radicals with doublet emission. *J. Appl. Phys.* **2021**, *129*, 180901.
2. Murto, P.; Bronstein, H., Electro-optical π-radicals: design advances, applications and future perspectives. *J. Mater. Chem. C* **2022**, *10*, 7368-7403.
3. Gao, S.; Cui, Z.; Li, F., Doublet-emissive materials for organic light-emitting diodes: exciton formation and emission processes. *Chem. Soc. Rev.* **2023**, *52*, 2875-2885.

4. Mizuno, A.; Matsuoka, R.; Mibu, T.; Kusamoto, T., Luminescent Radicals. *Chem. Rev.* **2024**, *124*, 1034-1121.

5. Quintes, T.; Mayländer, M.; Richert, S., Properties and applications of photoexcited chromophore–radical systems. *Nat. Rev. Chem.* **2023**, *7*, 75-90.

6. Schäfter, D.; Wischnat, J.; Tesi, L.; De Sousa, J. A.; Little, E.; McGuire, J.; Mas-Torrent, M.; Rovira, C.; Veciana, J.; Tuna, F.; Crivillers, N.; van Slageren, J., Molecular One- and Two-Qubit Systems with Very Long Coherence Times. *Adv. Mater.* **2023**, 2302114.

7. Gorgon, S.; Lv, K.; Grüne, J.; Drummond, B. H.; Myers, W. K.; Londi, G.; Ricci, G.; Valverde, D.; Tonnelé, C.; Murto, P.; Romanov, A. S.; Casanova, D.; Dyakonov, V.; Sperlich, A.; Beljonne, D.; Olivier, Y.; Li, F.; Friend, R. H.; Evans, E. W., Reversible spin-optical interface in luminescent organic radicals. *Nature* **2023**, *620*, 538-544.

8. Matsuoka, R.; Kimura, S.; Miura, T.; Ikoma, T.; Kusamoto, T., Single-Molecule Magnetoluminescence from a Spatially Confined Persistent Diradical Emitter. *J. Am. Chem. Soc.* **2023**, *145*, 13615-13622.

9. Ji, L.; Shi, J.; Wei, J.; Yu, T.; Huang, W., Air-Stable Organic Radicals: New-Generation Materials for Flexible Electronics? *Adv. Mater.* **2020**, *32*, 1908015.

10. Ratera, I.; Vidal-Gancedo, J.; Maspoch, D.; Bromley, S. T.; Crivillers, N.; Mas-Torrent, M., Perspectives for polychlorinated trityl radicals. *J. Mater. Chem. C* **2021**, *9*, 10610-10623.

11. Fox, M. A.; Gaillard, E.; Chen, C. C., Photochemistry of stable free radicals: the photolysis of perchlorotriphenylmethyl radicals. *J. Am. Chem. Soc.* **1987**, *109*, 7088-7094.

12. Hattori, Y.; Kusamoto, T.; Nishihara, H., Luminescence, Stability, and Proton Response of an Open-Shell (3,5-Dichloro-4-pyridyl)bis(2,4,6-trichlorophenyl)methyl Radical. *Angew. Chem. Int. Ed.* **2014**, *53*, 11845-11848.

13. Kimura, S.; Tanushi, A.; Kusamoto, T.; Kochi, S.; Sato, T.; Nishihara, H., A luminescent organic radical with two pyridyl groups: high photostability and dual stimuli-responsive

properties, with theoretical analyses of photophysical processes. *Chem. Sci.* **2018**, *9*, 1996-2007.

14. Kimura, S.; Uejima, M.; Ota, W.; Sato, T.; Kusaka, S.; Matsuda, R.; Nishihara, H.; Kusamoto, T., An Open-shell, Luminescent, Two-Dimensional Coordination Polymer with a Honeycomb Lattice and Triangular Organic Radical. *J. Am. Chem. Soc.* **2021**, *143*, 4329-4338.
15. Chen, L.; Arnold, M.; Blinder, R.; Jelezko, F.; Kuehne, A. J. C., Mixed-halide triphenyl methyl radicals for site-selective functionalization and polymerization. *RSC Adv.* **2021**, *11*, 27653-27658.
16. Coulson, C. A.; Rushbrooke, G. S., Note on the method of molecular orbitals. *Math. Proc. Camb. Phil. Soc.* **1940**, *36*, 193-200.
17. Dewar, M. J. S.; Longuet-Higgins, H. C., The Electronic Spectra of Aromatic Molecules I: Benzenoid Hydrocarbons. *Proc. Phys. Soc. A* **1954**, *67*, 795-804.
18. Longuet-Higgins, H. C.; Pople, J. A., The Electronic Spectra of Aromatic Molecules IV: Excited States of Odd Alternant Hydrocarbon Radicals and Ions. *Proc. Phys. Soc. A* **1955**, *68*, 591-600.
19. Castellanos, S.; Velasco, D.; López-Calahorra, F.; Brillas, E.; Julia, L., Taking Advantage of the Radical Character of Tris(2,4,6-trichlorophenyl)methyl To Synthesize New Paramagnetic Glassy Molecular Materials. *J. Org. Chem.* **2008**, *73*, 3759-3767.
20. Ai, X.; Evans, E. W.; Dong, S.; Gillett, A. J.; Guo, H.; Chen, Y.; Hele, T. J. H.; Friend, R. H.; Li, F., Efficient radical-based light-emitting diodes with doublet emission. *Nature* **2018**, *563*, 536-540.
21. Guo, H.; Peng, Q.; Chen, X.-K.; Gu, Q.; Dong, S.; Evans, E. W.; Gillett, A. J.; Ai, X.; Zhang, M.; Credgington, D.; Coropceanu, V.; Friend, R. H.; Brédas, J.-L.; Li, F., High stability and luminescence efficiency in donor–acceptor neutral radicals not following the Aufbau principle. *Nat. Mater.* **2019**, *18*, 977-984.

22. Abdurahman, A.; Hele, T. J. H.; Gu, Q.; Zhang, J.; Peng, Q.; Zhang, M.; Friend, R. H.; Li, F.; Evans, E. W., Understanding the luminescent nature of organic radicals for efficient doublet emitters and pure-red light-emitting diodes. *Nat. Mater.* **2020**, *19*, 1224-1229.

23. Murto, P.; Chowdhury, R.; Gorgon, S.; Guo, E.; Zeng, W.; Li, B.; Sun, Y.; Francis, H.; Friend, R. H.; Bronstein, H., Mesitylated trityl radicals, a platform for doublet emission: symmetry breaking, charge-transfer states and conjugated polymers. *Nat. Commun.* **2023**, *14*, 4147.

24. Mattiello, S.; Corsini, F.; Mecca, S.; Sassi, M.; Ruffo, R.; Mattioli, G.; Hattori, Y.; Kusamoto, T.; Griffini, G.; Beverina, L., First demonstration of the use of open-shell derivatives as organic luminophores for transparent luminescent solar concentrators. *Mater. Adv.* **2021**, *2*, 7369-7378.

25. Hattori, Y.; Kitajima, R.; Ota, W.; Matsuoka, R.; Kusamoto, T.; Sato, T.; Uchida, K., The simplest structure of a stable radical showing high fluorescence efficiency in solution: benzene donors with triarylmethyl radicals. *Chem. Sci.* **2022**, *13*, 13418-13425.

26. Arnold, M. E.; Kuehne, A. J. C., (2,6-Dichloro-4-iodophenyl)bis(2,4,6-trichlorophenyl)methane as a precursor in efficient cross-coupling reactions for donor and acceptor functionalized triphenylmethyl radicals. *Dyes Pigm.* **2023**, *208*, 110863.

27. Hattori, Y.; Kitajima, R.; Baba, A.; Yamamoto, K.; Matsuoka, R.; Kusamoto, T.; Uchida, K., Effects of hydrocarbon substituents on highly fluorescent bis(4-phenylphenyl)pyridylmethyl radical derivatives. *Mater. Adv.* **2023**, *4*, 5149-5159.

28. Bayliss, S. L.; Laorenza, D. W.; Mintun, P. J.; Kovos, B. D.; Freedman, D. E.; Awschalom, D. D., Optically addressable molecular spins for quantum information processing. *Science* **2020**, *370*, 1309-1312.

29. Laorenza, D. W.; Freedman, D. E., Could the Quantum Internet Be Comprised of Molecular Spins with Tunable Optical Interfaces? *J. Am. Chem. Soc.* **2022**, *144*, 21810-21825.

30. Englman, R.; Jortner, J., The energy gap law for radiationless transitions in large molecules. *Mol. Phys.* **1970**, *18*, 145-164.

31. Ishiyama, T.; Ishida, K.; Miyaura, N., Synthesis of pinacol arylboronates via cross-coupling reaction of bis(pinacolato)diboron with chloroarenes catalyzed by palladium(0)–tricyclohexylphosphine complexes. *Tetrahedron* **2001**, *57*, 9813-9816.

32. Chen, L.; Arnold, M.; Kittel, Y.; Blinder, R.; Jelezko, F.; Kuehne, A. J. C., 2,7-Substituted N-Carbazole Donors on Tris(2,4,6-trichlorophenyl)methyl Radicals with High Quantum Yield. *Adv. Optical Mater.* **2022**, *10*, 2102101.

33. Lu, C.; Cho, E.; Cui, Z.; Gao, Y.; Cao, W.; Brédas, J.-L.; Coropceanu, V.; Li, F., Towards Efficient and Stable Donor-Acceptor Luminescent Radicals. *Adv. Mater.* **2023**, *35*, 2208190.

34. Zhao, X.; Gong, J.; Alam, P.; Ma, C.; Wang, Y.; Guo, J.; Zeng, Z.; He, Z.; Sung, H. H. Y.; Williams, I. D.; Wong, K. S.; Chen, S.; Lam, J. W. Y.; Zhao, Z.; Tang, B. Z., A Simple Approach to Achieve Organic Radicals with Unusual Solid-State Emission and Persistent Stability. *CCS Chem.* **2022**, *4*, 1912-1920.

35. Kimura, S.; Kusamoto, T.; Kimura, S.; Kato, K.; Teki, Y.; Nishihara, H., Magnetoluminescence in a Photostable, Brightly Luminescent Organic Radical in a Rigid Environment. *Angew. Chem. Int. Ed.* **2018**, *57*, 12711-12715.

36. Liu, C.-H.; Hamzehpoor, E.; Sakai-Otsuka, Y.; Jadhav, T.; Perepichka, D. F., A Pure-Red Doublet Emission with 90 % Quantum Yield: Stable, Colorless, Iodinated Triphenylmethane Solid. *Angewandte Chemie International Edition* **2020**, *59*, 23030-23034.

37. Kato, K.; Kimura, S.; Kusamoto, T.; Nishihara, H.; Teki, Y., Luminescent Radical-Excimer: Excited-State Dynamics of Luminescent Radicals in Doped Host Crystals. *Angewandte Chemie International Edition* **2019**, *58*, 2606-2611.

38. Kimura, S.; Kimura, S.; Kato, K.; Teki, Y.; Nishihara, H.; Kusamoto, T., A ground-state-dominated magnetic field effect on the luminescence of stable organic radicals. *Chem. Sci.* **2021**, *12*, 2025-2029.

39. Burks, S. R.; Makowsky, M. A.; Yaffe, Z. A.; Hoggle, C.; Tsai, P.; Muralidharan, S.; Bowman, M. K.; Kao, J. P. Y.; Rosen, G. M., The Effect of Structure on Nitroxide EPR Spectral Linewidth. *J. Org. Chem.* **2010**, *75*, 4737-4741.

40. Bobet, A.; Cuadrado, A.; Fajarí, L.; Sirés, I.; Brillas, E.; Almajano, M. P.; Jankauskas, V.; Velasco, D.; Juliá, L., Bipolar charge transport in organic electron donor-acceptor systems with stable organic radicals as electron-withdrawing moieties. *J. Phys. Org. Chem.* **2019**, *32*, e3974.

41. Bowman, M. K.; Mailer, C.; Halpern, H. J., The solution conformation of triarylmethyl radicals. *J. Magn. Reson.* **2005**, *172*, 254-267.

42. Grimme, S.; Antony, J.; Ehrlich, S.; Krieg, H., A consistent and accurate ab initio parametrization of density functional dispersion correction (DFT-D) for the 94 elements H-Pu. *J. Chem. Phys.* **2010**, *132*, 154104.

43. St. John, P. C.; Guan, Y.; Kim, Y.; Etz, B. D.; Kim, S.; Paton, R. S., Quantum chemical calculations for over 200,000 organic radical species and 40,000 associated closed-shell molecules. *Sci. Data* **2020**, *7*, 244.

44. Lu, T.; Chen, F., Multiwfn: A multifunctional wavefunction analyzer. *J. Comput. Chem.* **2012**, *33*, 580-592.

45. Humphrey, W.; Dalke, A.; Schulten, K., VMD: Visual molecular dynamics. *J. Mol. Graphics* **1996**, *14*, 33-38.

46. Stoll, S.; Schweiger, A., EasySpin, a comprehensive software package for spectral simulation and analysis in EPR. *J. Magn. Reson.* **2006**, *178*, 42-55.

47. Sheldrick, G., SHELXT - Integrated space-group and crystal-structure determination. *Acta Cryst.* **2015**, *A71*, 3-8.

48. Sheldrick, G., Crystal structure refinement with SHELXL. *Acta Cryst.* **2015**, *C71*, 3-8.

49. Macrae, C. F.; Edgington, P. R.; McCabe, P.; Pidcock, E.; Shields, G. P.; Taylor, R.; Towler, M.; van de Streek, J., Mercury: visualization and analysis of crystal structures. *J. Appl. Cryst.* **2006**, *39*, 453-457.

50. Macrae, C. F.; Bruno, I. J.; Chisholm, J. A.; Edgington, P. R.; McCabe, P.; Pidcock, E.; Rodriguez-Monge, L.; Taylor, R.; van de Streek, J.; Wood, P. A., Mercury CSD 2.0 - new features for the visualization and investigation of crystal structures. *J. Appl. Cryst.* **2008**, *41*, 466-470.

For Table of Contents Only